CrossMark

ORIGINAL PAPER

Alizarin red: a reactive dye to enhance nanoengineered polypyrrole with high electrochemical energy storage

Limin Zang[1,2] · Qifan Liu[1] · Chao Yang[1,3] (iD) · Jian Chen[1] · Jianhui Qiu[2] · Ge Song[1]

Abstract High-performance supercapacitors require the molecular-level linkage of charge transport components and charge-storage components. In this work, polypyrrole (PPy) was prepared via in situ chemical oxidative polymerization in the presence of a reactive dye (alizarin red S, ARS) which could play the role of both dopant and physical cross linker for pyrrole polymerization. The effects of ARS concentration on morphology, structure, electrical conductivity, and electrochemical performance were studied. When the feeding ratio of pyrrole: ARS was 2:1, the as-prepared ARS-doped PPy sample exhibited a high-mass-specific capacitance of 319 F/g at a current density of 1.0 A/g. All PPy–ARS electrodes possessed excellent capacitance retention. Especially, the specific capacitance of the sample with the highest ARS content increased by 18% of its initial value after 2000 cycles. The results demonstrated that the multifunctional dye ARS could effectively improve the performances of PPy as an electrode material for supercapacitors.

**Keywords** Alizarin red · Conducting polymer · Supercapacitor · Anthraquinone · Redox

✉ Chao Yang
   yangchao_chem@163.com

1   State Key Laboratory Breeding Base of Nonferrous Metals and Specific Materials Processing, College of Material Science and Engineering, Guilin University of Technology, Guilin 541004, China

2   Department of Machine Intelligence and Systems Engineering, Faculty of Systems Science and Technology, Akita Prefectural University, Akita 015-0055, Japan

3   Key Laboratory of Biomass Chemical Engineering of Ministry of Education, Zhejiang University, Hangzhou 310027, China

Introduction

Electrochemical capacitors are attractive energy storage devices that fill the gap between batteries and traditional dielectric capacitors. They can be classified into two types depending on the charge-storage mechanism, known as electrochemical double-layer capacitors and redox supercapacitors [1–3]. As a new class of materials, conducting polymers possess the electrical, optical, electronic, and magnetic properties of metals, as well as the processability and mechanical properties of the conventional polymers [4–7]. Among the various conducting polymers, polypyrrole (PPy) is one of the most promising materials for electrical applications, including polymer electrodes [8], electromagnetic interference shielding films [9, 10], sensors [11], electroactive polymer actuators [12, 13], and all-plastic conductive composites [14]. In recent years, there have been many researches focusing on the performances of PPy and its composites in the field of energy storage. Compared with metal oxide electrodes, PPy has several merits such as low cost, low toxicity, easy preparation, low density, and high electrical conductivity. However, PPy and other conducting polymers suffer from the inherent drawbacks of limited specific capacity and poor stability upon repeated cycling, causing nucleophilic attack of other species on the polymer matrix and gradual degradation in the mechanical strength during the charge–discharge process [15]. The integration of molecular components into conductive composites is a facile approach for addressing functional molecules on the macroscopic level. One promising synthetic route is the "wiring" of electroactive molecules to conducting polymers (CPs), leading to composite materials which bring together the properties of both components [16]. The extremely high electronic charge density of 1787 C/g or 496 mAh/g for hydroquinone that two electrons and protons are stored in its 6 carbon and 2 oxygen atoms is more favorable than the standard electrochemical systems [17]. Hence, taking advantage of the quinone redox characteristic in electroactive materials to enhance charge-storage capacity is satisfying. For instance, researchers have prepared interpenetrating networks of PPy with lignosulfonate which is a water-soluble anionic polymer containing quinone units and investigated their charge-storage capacity due to quinone electrochemistry [18]. However, lignosulfonate impeded electron transfer between PPy chains, leading to higher resistivity of PPy. Using the small redox active molecules may solve above problem [19, 20]. Furthermore, some dopants can afford conducting polymers with satisfactory thermal stability, high conductivity, good electrochemical performance,

Fig. 1 Molecular structure of ARS reactive dye (3, 4-dihydroxy anthraquinone-2-sulfonate)
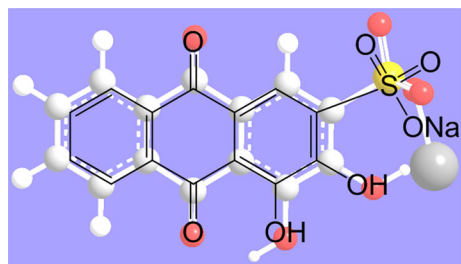
and special morphology [21–24]. Alizarin red S (ARS, Fig. 1) is an anthraquinone derivative that possesses redox function. It is desirable to be used to increase the charge-storage capacity. In particular, because of the multiple sulfonate groups of ARS and strong interactions between PPy and ARS, it is also expected to be used as dopant to improve the electrochemical performance and stability during the charge–discharge process of PPy. Besides, ARS would exert π–π stacking with PPy, which play a part in enhancing the electrochemical capacities of PPy in this work. The morphology, structure, and electrical properties of the resultant PPy–ARS composites were characterized by transmission electron microscope (TEM), Fourier transform infrared spectroscopy (FTIR), X-ray photoelectron spectroscopy (XPS), X-ray diffraction (XRD), cyclic voltammetry (CV), and galvanostatic charge–discharge test.

Experimental section

Materials

Pyrrole, ammonium persulfate (APS), and Alizarin red S sodium salt (ARS) were purchased from Nacalai Tesque, Inc., Japan. Pyrrole monomer dehydrated with calcium hydride for 24 h was distilled under reduced pressure before use. All solutions were prepared with deionized water. All other chemicals were reagent quality.

Preparation of ARS-enhanced PPy

The ARS-enhanced PPy (PPy–ARS) was prepared via in situ oxidative polymerization method. Typically, a certain amount of ARS was added to 100 mL of deionized water in a 250 mL round-bottom flask and stirred for 15 min. Freshly distilled pyrrole (1 mL, 14.4 mmol) was added to the above solution and stirred in ice-water bath for 30 min to obtain a pale yellow solution. Then, an aqueous solution (20 mL) of APS (0.90 g, 3.9 mmol) was added dropwise to this mixture to initiate the oxidative polymerization. The reaction was continued for 10 h in the ice-cold condition under mechanical stirring and nitrogen atmosphere. The resulting precipitates were filtrated off and washed with deionized water several times until filtrate turned colorless. Finally, the product was dried in vacuum at 50 °C for 24 h to obtain the desired PPy as a dark powder. The detailed conditions of the polymerizations are given in Table 1.

Characterizations and electrochemical measurements

The morphology of the samples was investigated with a transmission electron microscope (TEM, JSM-2010HR) at an accelerating voltage of 5 kV. The Fourier transform infrared spectroscopy (FTIR) measurements (Nicolet Impact 400) were carried out with the KBr pellet method. Thermogravimetric results were obtained using a TA Instrument Q500 thermogravimetric analyzer at a heating rate of 10 °C/

Table 1 Compositions of PPy–ARS investigated in this work

Sample	Pyrrole (mL)	ARS (mg)	APS (g)	Conductivity (S/m)	Particle size (nm)	Yield (%)
S-1	1	51.0	0.9	830	Aggregation	79.6
S-2	1	167.7	0.9	2000	80	72.1
S-3	1	415.3	0.9	830	50	65.7
S-4	1	969.1	0.9	230	90	47.3

min from 50 to 800 °C under nitrogen atmosphere. X-ray photoelectron spectroscopy (XPS) measurements were performed on a PHI 5000 Series (Shimadzu, Japan) equipped with a monochromatic MgK_α X-ray source and a resistive anode detector. The electrical conductivities of the samples were measured using SDY-4 Four-Point Probe Meter (Guangzhou Semiconductor Material Academe) at ambient temperature. Electrochemical experiments were performed on a CHI660D electrochemical workstation (Shanghai, China) with a conventional three-electrode system. The working electrode was prepared by mixing 80 wt% active material with 15 wt% acetylene black and 5 wt% polyvinylidene fluoride. A platinum foil and a saturated calomel electrode (SCE) were used as the counter and reference electrode, respectively. Cyclic voltammetry was performed in the voltage range of − 1.0–0.6 V at a scan rate of 10 mV/s. Galvanostatic charge–discharge experiments were carried out in the potential range from − 1.0 to 0.6 V with an applied current density of 1.0 A/g.

Results and discussion

Morphology observations

Figure 2 shows the TEM images of PPy–ARS samples. Basically, PPy shows a granular-like morphology with a nanoscale. The use of reactive dye ARS as dopant led to a significant decrease in particle size. TEM images of the samples clearly indicated that the obtained products were uniform nanoparticles and the average diameter of S-2, S-3, and S-4 was, respectively, about 80, 50 and 90 nm, whereas S-1 showed serious aggregation. It should be ascribed to the fact that the presence of ARS which contains phenolic hydroxyl, anthraquinonyl, and sulfonate groups leads to the hydrophilic surface and facilitates reduction of particle size. From the viewpoint of pseudocapacitive electrode materials, the resulting PPy–ARS composite with smaller particle size is desirable, since it enables more surface active sites for redox reactions which should be conducive to achieving higher specific capacitance. However, excessive intake of ARS led to aggregation of PPy particles via hydrogen bonds.
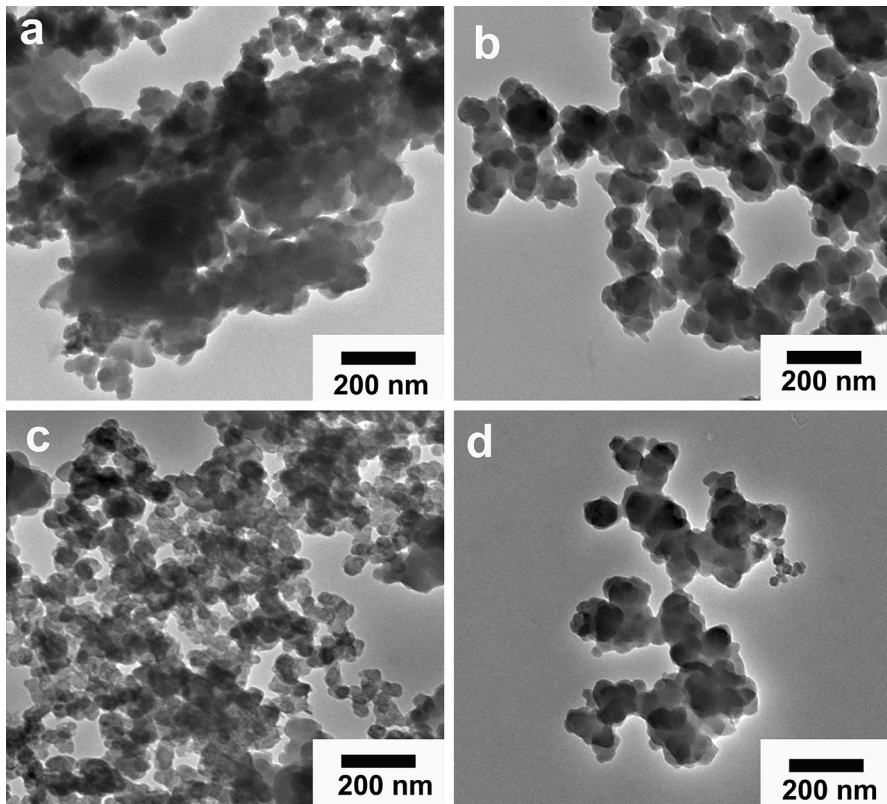
Fig. 2 TEM images of the PPy–ARS samples (**a** S-1, **b** S-2, c S-3, and **d** S-4)

FTIR Analysis

The FTIR spectra of PPy, ARS, and PPy–ARS samples are shown in Fig. 3. For PPy, the peaks at 1540 and 1455/cm were associated with the C=C– and C–N-stretching vibration in the pyrrole ring [25, 26]. The peaks presented at 1300 and 785/cm were due to C–H in-plane deformation and C–H wagging vibration, respectively. In the FTIR spectrum of ARS, the bands observed at 1637 and 1668/cm were assigned to C=O-stretching vibration, where the peak at low wavenumber referred to intramolecular hydrogen bonding between C=O and –OH. The peak of aromatic C=C-stretching vibration appeared at 1590/cm. The asymmetrical and symmetrical stretching vibrations of SO_3 in the form of RSO_3Na were observed at 1160 and 1065/cm, respectively [27]. For PPy–ARS samples, both the characteristic peaks of PPy and ARS appeared, which indicated that PPy was doped with ARS. It is important to clarify how ARS is incorporated into PPy. The asymmetrical stretching vibrations of SO_3 in PPy–ARS samples shifted to 1167/cm which overlapped with the peak of PPy at 1178/cm. The symmetrical stretching vibrations of SO_3 in PPy–ARS samples shifted to 1086/cm, indicating the interaction between RSO_3^- and doped PPy. Moreover, the intensity for the
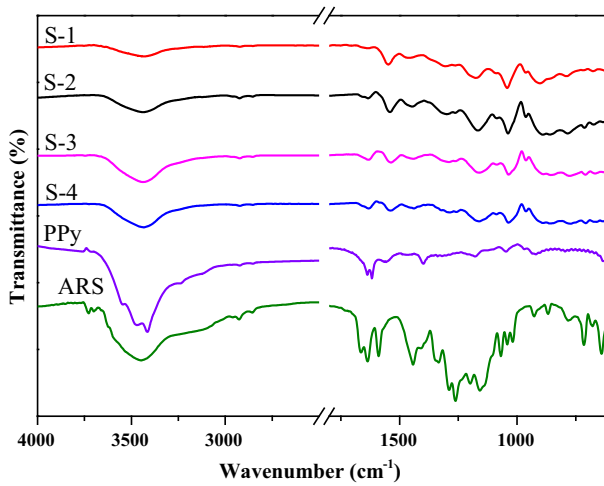
Fig. 3 FTIR spectra of ARS, PPy, and ARS–PPy samples

1086/cm absorption band increased in PPy–ARS samples as the feeding ratio of ARS increased. It showed that the content of ARS played a significant role in the interactions between PPy and ARS.

X-ray photoelectron spectroscopy

X-ray photoelectron spectroscopy (XPS) was used to determine the content of the dopant as well as the doping level of the resulting PPy–ARS samples [28]. Figure 4
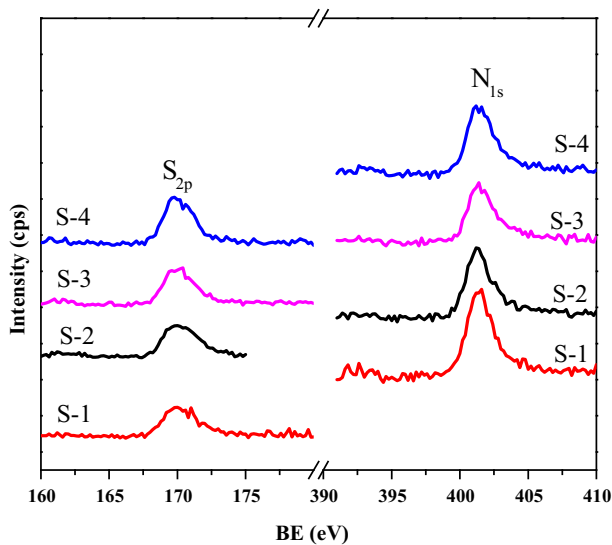

Fig. 4 N1s and S2p XPS spectra of ARS–PPy samples

shows high-resolution N1 s and S2p spectra for PPy–ARS samples. The S/N ratio of S-1 to S-4 was 0.228, 0.286, 0.392, and 0.401, respectively, which was agreed with the data of the elemental analysis. The increased S/N ratio indicated that there was an increase in the doping level as the feeding ratio of ARS was increased. It is known that 25–30 mol% of PPy moiety is generally doped when it is synthesized by chemical polymerization [29]. However, the S/N ratio of S-4 was about 0.4, which was assumed that the effective doping level of the PPy–ARS should be lower than its apparent doping level, even though the apparent doping level increased with the increasing feeding ratio of ARS. Excessive amounts of ARS interacted with PPy through the formation of hydrogen bonds between the PPy secondary amine groups and carbonyls or the hydroxyl groups present in ARS.

XRD analysis

The XRD studies of PPy–ARS samples are shown in Fig. 5. In general, PPy is an amorphous polymer, because its linear rigid chains cannot fold to induce crystalline domain [30]. When PPy was doped with ARS, PPy tended to arrange into a three-dimensional ordered fashion. To be specific, for PPy–ARS samples, the peak at $2\theta = 26.2$, which depended on the doping level and reflected pyrrole–pyrrole interplanar distance [31], became sharper as the feeding ratio of ARS increased. This indicated that the decrease in the feeding amount of ARS decreases the interplanar distance in the ARS dope PPy and produces a rather ordered PPy.

Electrical conductivity and electrochemical performance of PPy–ARS

Table 1 reflects the variation of electrical conductivity as a function of feeding ratio of ARS. The obtained maximum electrical conductivity was 2000 S/m, which was
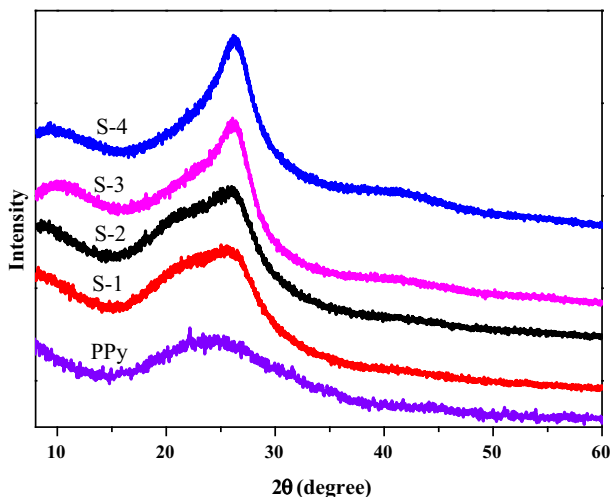

Fig. 5 X-ray diffraction patterns of PPy and ARS–PPy samples

comparable with values for similar sulfuric-acid-doped PPy reported in the literatures [32–35]. With the increase in the ARS content, the electrical conductivity of the sample first increased and then decreased. There are two primary reasons for this phenomenon: first, the organic sulfonate is an effective dopant for conjugated conducting polymers. Namely, doping of PPy with ARS can cause the change of electron density of pyrrole ring in the polymer backbone. It is useful for improving the conductivity of PPy. On the other hand, ARS, containing no free electrons, is a poor conductor of electricity. This means that the incorporation of ARS has a negative effect on improving the conductivity of PPy. Therefore, the two opposing effects of ARS are responsible for the changing trend of electrical conductivity of PPy–ARS with different feeding ratios of ARS.

To further evaluate the applicability of the PPy–ARS in electrochemical energy storage devices, the cycling performance and galvanostatic charge–discharge performance of the PPy–ARS samples were investigated in a three-electrode system. Figure 6 shows the CV curves of the samples performed at a scan rate of 10 mV/s in 1.0 mol/L KCl solution. In the potential range of − 1.0–0.6 V, the PPy–ARS electrode showed a typical pseudocapacitive profile and the reversible redox peaks were associated with oxidation–reduction processes of hydroanthraquinone/anthraquinone groups present in ARS, confirming the successful incorporation of ARS into the composite [36, 37]. The incorporation of different contents ARS in the PPy matrix significantly influenced the specific capacitance, as indicated by important differences in cyclic voltammograms. Among the samples, S-3 showed the highest output current and largest area, indicating the best charge transport properties and specific capacitance.

Galvanostatic charge–discharge curves of PPy–ARS electrodes with different contents of ARS were recorded (Fig. 7) at a current density of 1.0 A/g within the
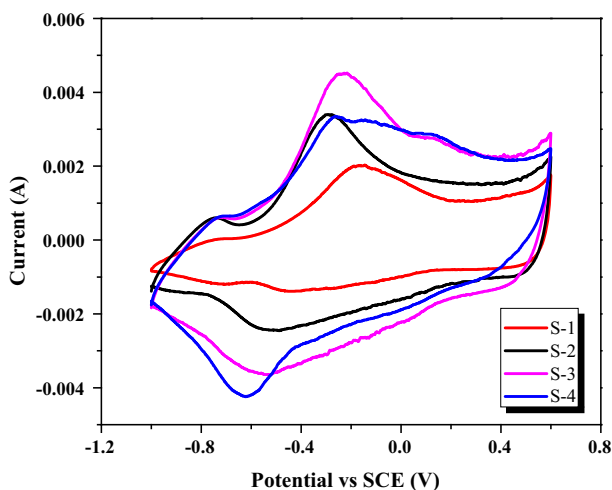

Fig. 6 CVs of PPy–ARS samples in 1.0 M KCl solution recorded at scan rate of 10 mV/s
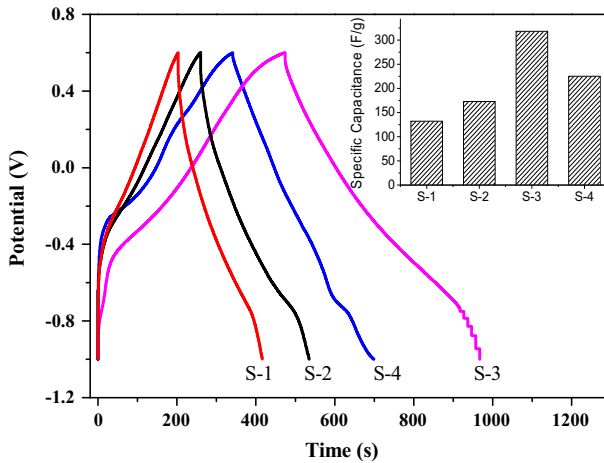
Fig. 7 Galvanostatic charge–discharge curves of PPy–ARS nanocomposite electrodes at a current density of 1.0 A/g in 1 M KCl solution

potential window from -1.0 to 0.6 V. The specific capacitance (C_m) can be calculated from the equation [38]:

$$C_m = (I \times t)/m \times V,$$

where I is the charge–discharge current, t is the discharge time, V is the potential drop during discharge, and m is the mass of active material. The C_m values of S-1–S-4 calculated at a current density of 1.0 A/g were 132, 173, 317, and 255 F/g, respectively. On one hand, with the increasing of ARS, the doping level of the PPy and the electrical conductivity of the PPy–ARS nanocomposite increased. In addition, as the content of ARS increased, the decreasing particle size can shorten the ion-diffusion length. Based on these, the capacitance increased first. On the other hand, with a further increasing of ARS, it increased resistance of carriers in the conjugated chains, resulting in a decreased capacitance. To obtain more information about the ability of PPy–ARS samples to function as electrodes in supercapacitors, an EIS experiment was carried out in a 1.0 M KCl solution at open-circuit potential (Fig. 8). In the medium–low-frequency region, an unequal semicircular pattern can be discovered in both curves. At low frequency, the impedance plots exhibited a vertical line, indicating a limiting diffusion process in the electrolyte.

The long-term cycle stability was tested by galvanostatic charge–discharge at a current density of 1.0 A/g for 2000 cycles and the result is shown in Fig. 9. The capacitance of the supercapacitor with PPy–ARS nanocomposite electrodes increased in the first 100 cycles due to the self-activation process, and then gradually decreased in the following cycles. It is inferred that the hydroxyl, anthraquinonyl, and sulfonate groups existing in ARS could not only play the role as dopant, but also crosslinking agent through physical crosslinking of PPy via hydrogen bonds. The schematic representation of doping and physical crosslinking mechanism is illustrated in Fig. 10. Such structure is not beneficial for the
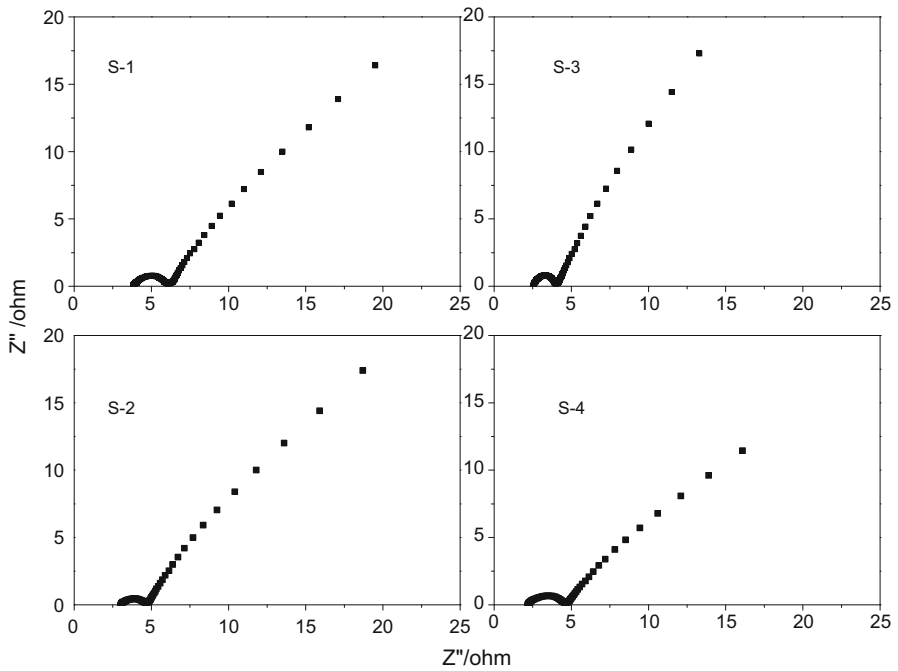
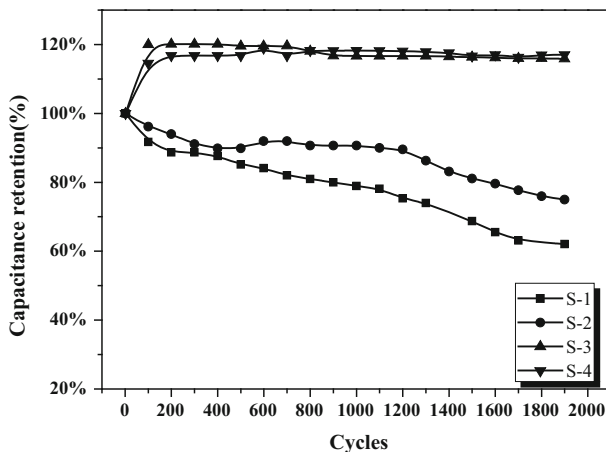**Fig. 8** Impedance Nyquist plots of the PPy–ARS samples

Fig. 9 Cycle-life performance of the ARS–PPy sample at a current density of 1.0 A/g in 1.0 M KCl solution

diffusivity of electrolyte so as to make the nanocomposite possess self-activation process behavior. No significant self-activation process was observed in the samples with low content of ARS. It is further evidenced that excessive ARS could offer physical crosslinking via hydrogen bonds. All the samples kept the capacitance very
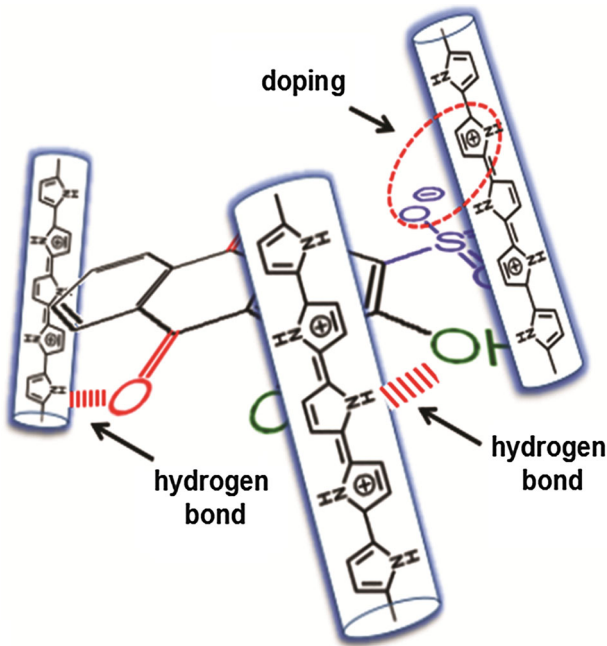
Fig. 10 Schematic representation for mechanism of interaction between PPy and ARS

well after cycling for 2000 times. It is especially noteworthy that the more ARS in samples the better long-term cycle stability they were. All the samples showed good capacitance retention after cycling 2000 times. It is notable that the more ARS in samples the better long-term cycle stability they were. When the content ARS was relatively low, the capacitance retention showed a decreased trend (S-1 and S-2), whereas the samples with relatively high ARS content even exhibited an increased capacitance compared with its initial value after 2000 cycles (S-3 and S-4).

Conclusion

In summary, we have successfully fabricated highly conductive PPy–ARS nanocomposites by in situ chemical oxidative polymerization. The ARS would exert π–π stacking with PPy, which played a part in improving the conductivity and electrochemical capacities of PPy–ARS. The specific capacity of the PPy–ARS was significantly enhanced by anthraquinone sulfonate as a dopant and C_m of S-3 sample reached 317 F/g. Moreover, the PPy–ARS supercapacitor exhibited a good electrochemical stability without the capacitance degradation over 2000 cycles. The corporation of ARS can thus considerably improve the performances of PPy and provide a suitable preparation for conjugated polymer-based materials.

References

1. Xiao FS, Yang Z, Zhang H et al (2015) Scalable synthesis of freestanding sandwich-structured graphene/polyaniline/graphene nanocomposite paper for flexible all-solid-state supercapacitor. Sci Rep 5:9359
2. Radja I, Djelad H, Morallon E et al (2015) Characterization and electrochemical properties of conducting nanocomposites synthesized from *p*-anisidine and aniline with titanium carbide by chemical oxidative method. Synth Met 202:25–32
3. Chouli F, Zehhaf A, Benyoucef A (2014) Preparation and characterization of the new conducting composites obtained from 2-methylaniline and Aniline with activated carbon by in situ intercalative oxidative polymerization. Macromol Res 22:26–31
4. Tang H, Wang J, Yin H (2015) Growth of polypyrrole ultrathin films on MoS2 monolayers as high-performance supercapacitor electrodes. Adv Mater 27:1117–1123
5. Benykhlef S, Bekhoukh A, Berenguer R et al (2016) PANI-derived polymer/Al_2O_3 nanocomposites: synthesis, characterization, and electrochemical studies. Colloid Polym Sci 294:1877–1885
6. Gürbüz O, Filiz B, Orhan Ş et al (2016) Structural, optical and electrical properties of polypyrrole in an ionic liquid. Polym Bull. doi:10.1007/s00289-016-1856-3
7. Dahou FZ, Khaldi MA, Zehhaf A et al (2016) Nanocomposite of 2-aminophenol with aniline using copper-montmorillonite: synthesis, characterization, conductivity, and electrochemical study. Adv Polym Tech 35:411–418
8. Davoglio RA, Biaggio SR, Bocchi N et al (2013) Flexible and high surface area composites of carbon fiber, polypyrrole, and poly (DMCT) for supercapacitor electrodes. Electrochim Acta 93:93–100
9. Zhao H, Hou L, Lu Y (2016) Electromagnetic shielding effectiveness and serviceability of the multilayer structured cuprammonium fabric/polypyrrole/Copper (CF/PPy/Cu) composite. Chem Eng J 297:170–179
10. Kim YY, Yun J, Kim HI et al (2012) Effect of oxyfluorination on electromagnetic interference shielding of polypyrrole-coated multi-walled carbon nanotubes. J Ind Eng Chem 18:392–398
11. Lee JS, Jun J, Shin DN et al (2014) Urchin-like polypyrrole nanoparticles for highly sensitive and selective chemiresistive sensor application. Nanoscale 6:4188–4194
12. Okuzaki H, Kuwabara T, Funasaka K, Saido T (2013) Humidity-sensitive polypyrrole films for electro-active polymer actuators. Adv Funct Mater 23:4400–4407
13. Zheng WG, Alici R, Clingan BJ et al (2013) Polypyrrole stretchable actuators. J Polym Sci Pol Phys 51:57–63
14. Yang C, Zang LM, Qiu JH et al (2014) Nano-Cladding of natural microcrystalline cellulose with conducting polymer: preparation, characterization, and application in energy storage. RSC Adv 4:40345–40351
15. Lang XQ, Wan C, Feng X et al (2010) The role of anthraquinone sulfonate dopants in promoting performance of polypyrrole composites as pseudo-capacitive electrode materials. Synth Met 160:1800–1804
16. Herrmann S, Aydemir N, Nägele F et al (2017) Enhanced capacitive energy storage in polyox-ometalate-doped polypyrrole. Adv Funct Mater. doi:10.1002/adfm.201700881
17. Milczarek G, Inganas O (2012) Renewable cathode materials from biopolymer/conjugated polymer interpenetrating networks. Science 335:1468–1471
18. Yang C, Liu P (2009) Water-dispersed conductive polypyrroles doped with lignosulfonate and the weak temperature dependence of electrical conductivity. Ind Eng Chem Res 48:9498–9503
19. Halls JE, Ahn SD, Jiang D et al (2013) Proton uptake vs. redox driven release from metal-organic-frameworks: alizarin red s reactivity in Umcm-1. J Electroanal Chem 689:168–175
20. Zhu Y, Shi K, Zhitomirsky I (2014) Anionic dopant-dispersants for synthesis of polypyrrole coated carbon nanotubes and fabrication of supercapacitor electrodes with high active mass loading. J Mater Chem A 2:14666–14673
21. Zang LM, Qiu JH, Yang C et al (2015) Enhanced conductivity and electrochemical performance of electrode material based on multifunctional dye doped polypyrrole. J Nanosci Nanotechnol 16:2564–2570

22. Yalçınkaya S, Demirbilek C, Özdemir Dinç C (2015) Preparation and characterization of poly-pyrrole/dextran sulphate composite: its electrochemical and thermal behaviors. Polym Bull 72:2843–2855
23. Lang XQ, Wan C, Feng X et al (2010) The role of anthraquinone sulfonate dopants in promoting performance of polypyrrole composites as pseudo-capacitive electrode materials. Synth Met 160:1800–1804
24. Wan QY, Fan SS, Yue XJ et al (2010) Improved capacitive performance of polypyrrole doped with 9,10-anthraquinone-2-sulfonic acid sodium salt. Acta Phys Chim Sin 26:2951–2956
25. Sun W, Zhou Y, Su Q et al (2016) Removal Of chromium (VI) from aqueous solutions using polypyrrole-based magnetic composites. Polym Bull. doi:10.1007/s00289-016-1769-1
26. Zang LM, Qiu JH, Yang C et al (2015) In situ preparation of polypyrrole nanorod composite in the presence of phosphorylated polyvinyl alcohol. Adv Polym Technol. doi:10.1002/adv.21497
27. Moriguchi T, Yano K, Nakagawa N et al (2003) Elucidation Of adsorption mechanism of bone-staining agent alizarin red s on hydroxyapatite by Ft–Ir microspectroscopy. J Colloid Interface Sci 260:19–25
28. Moulder JF (1995) Handbook of X-ray photoelectron spectroscopy: a reference book of standard spectra for identification and interpretation of xPS data. Physical Electronics, Chanhassen, pp 40–56
29. Kim DY, Lee JY, Kim CY et al (1995) Difference in doping behavior between polypyrrole films and powders. Synth Met 72:243–248
30. Mondal S, Sangaranarayanan MV (2015) A novel, rapid synthetic protocol for controllable sizes, conductivities and monomer units of soluble polypyrrole. Eur Polym J 71:596–611
31. Luo JJ, Lu QF (2015) Controllable preparation and heavy-metal-ion adsorption of lignosulfonate-polypyrrole composite nanosorbent. Polym Compos 36:1546–1556
32. Xing S, Zhao G (2006) Morphology And thermostability of polypyrrole prepared from SDBS aqueous solution. Polym Bull 57:933–943
33. Taunk M, Kapil A, Chand S (2011) Chemical synthesis and low temperature electrical transport in polypyrrole doped with sodium bis(2-ethylhexyl) sulfosuccinate. J Mater Sci Mater Electron 22:136–142
34. Omastova M, Trchova M, Pionteck H et al (2004) EFfect of polymerization conditions on the properties of polypyrrole prepared in the presence of sodium bis(2-ethylhexyl) sulfosuccinate. Synth Met 143:153–161
35. Yang C, Wang X, Wang Y et al (2012) Polypyrrole nanoparticles with high dispersion stability via chemical oxidative polymerization in presence of an anionic–non-ionic bifunctional polymeric sur-factant. Powder Technol 217:134–139
36. Algharaibeh Z, Liu X, Pickup PG (2009) An asymmetric anthraquinone-modified carbon/ruthenium oxide supercapacitor. J Power Sources 187:640–643
37. Kalinathan K, DesRoches DP, Liu X et al (2008) Anthraquinone modified carbon fabric superca-pacitors with improved energy and power densities. J Power Sources 181:182–185
38. Bard AJ, Fualkner LR (2000) Electrochemicalmethods: fundamentals and applications, 2nd edn. Wiley, Hoboken